arXiv:1311.5891v1 [hep-ph] 22 Nov 2013

Improving Higgs plus Jets analyses through Fox–Wolfram Moments

Catherine Bernaciak,[1] Bruce Mellado,[2] Tilman Plehn,[1] Peter Schichtel,[1] and Xifeng Ruan[2]

[1] *Institut für Theoretische Physik, Universität Heidelberg, Germany*
[2] *School of Physics, University of the Witwatersrand, Johannesburg, South Africa*

It is well known that understanding the structure of jet radiation can significantly improve Higgs analyses. Using Fox–Wolfram moments we systematically study the geometric patterns of additional jets in weak boson fusion Higgs production with a decay to photons. First, we find a significant improvement with respect to the standard analysis based on an analysis of the tagging jet correlations. In addition, we show that replacing a jet veto by a Fox-Wolfram moment analysis of the extra jet radiation almost doubles the signal-to-background ratio. Finally, we show that this improvement can also be achieved based on a modified definition of the Fox–Wolfram moments which avoids introducing a new physical scale below the factorization scale. This modification can reduce the impact of theory uncertainties on the Higgs rate and couplings measurements.

Contents

I. Introduction 2

II. Setting the Stage 3
A. Fox–Wolfram moments 3
B. Event generation 4
C. Boosted decision trees 4

III. Tagging jet correlation 5

IV. Replacing a jet veto 6

V. Avoiding new scales 9

VI. Outlook 10

References 11

I. INTRODUCTION

After the recent Higgs discovery by ATLAS and CMS [1–3], the careful and systematic study of Higgs properties is becoming a key research program at the LHC and a future linear collider [4]. The theoretical implications of the first fundamental scalar particle include many open questions, including the actual generation of a vacuum expectation value, the stability of its physical mass, or the link between the Higgs potential at the weak scale to high–scale structures [5]. In the language of quantum field theory we need to construct the weak–scale Higgs Lagrangian including the operator basis and the corresponding couplings [6].

At the LHC the weak boson fusion production channel (WBF) [7–11] plays an important role in answering some of these question, in particular once the LHC runs closer to its design energy. It allows us to directly probe the unitarization of $WW \to WW$ scattering and carries information on tree–level Higgs couplings with negligible impact of perturbative extensions of the Standard Model. Experimentally, two forward tagging jets are highly effective in reducing QCD backgrounds [12], which means that Higgs analyses in weak boson fusion typically benefit from a signal–to–background ratio around unity.

As an analysis tool utilizing the unique QCD structure of weak boson fusion we rely on a central jet veto [13–18]. It is based on the fact that we can generate large logarithms and increase central jet radiation in QCD backgrounds while leaving the jet activity in the signal at low level. This shift from staircase scaling of jets (with constant ratios between successive exclusive jet bins) in signal and background to staircase scaling in the signal and Poisson scaling in the background can be derived from first–principles QCD [13]. The resulting jet veto survival probabilities for the the QCD backgrounds can be measured in data. Their calculation from QCD is plagued with significant theory uncertainties which in turn will soon dominate the extraction of the Higgs couplings at the LHC [6]. In addition, a jet veto always removes a wealth of kinematic information carried by these jets, so the question arises whether the information from the jets recoiling against the Higgs cannot be used more efficiently.

To answer the question of how much information is encoded in the jet activity of Higgs candidate events we need to systematically study multi-jet kinematics. For example in flavor physics Fox–Wolfram moments (FWM) are an established tool to analyze such geometric patterns [19], but they have hardly been employed by the ATLAS and CMS collaborations. By construction, they are particularly well suited to study the geometry of tagging jets in weak boson fusion [20]. Dependent on the specific construction of their weights the moments can also be sensitive measures of the additional jet activity in an event. Ideally, they will enhance a central jet veto defined on a fixed phase space region to some kind of weighted jet veto over phase space regions based on the kinematics of the hard process. Moreover, by choosing different weights the moments can be adjusted such that they avoid introducing a fixed scale below the factorization scale of the hard process. At the expense of the background rejection efficiency they can be tuned to introduce smaller theory uncertainties. This will allow the ATLAS and CMS experiments to optimize their Higgs analyses including theory uncertainties and significantly improve the case for a luminosity upgrade based on Higgs couplings measurements.

In this paper we will attempt to answer three questions based on the weak boson fusion analysis with a Higgs decay to photons. This includes a study of the signal process, the Higgs background from gluon fusion, and the continuum production of a photon pair with jets:

1. in Section III we will apply Fox–Wolfram moments to the kinematics of the two tagging jets only. Based on a multivariate analysis we will estimate how much these additional observables can improve the current ATLAS results at 8 TeV collider energy.

2. in Section IV we will compare the performance of a set of Fox–Wolfram moments with a specific (unit) weight in comparison to the usual central jet veto for the 13 TeV run. Moreover, a multivariate analysis of Fox-Wolfram moments allows us to define a ROC curve with a free choice of operating points.

3. in Section V we will introduce a new weight in the Fox–Wolfram moments. It avoids introducing a physical momentum scale for the jet veto which lies below the factorization scale.

Obviously, our conclusions are immediately applicable to ongoing and future LHC analyses. Fox–Wolfram moments have been tested in a few ATLAS and CMS analyses, so it should be a simple task to also include them in Higgs analyses.

II. SETTING THE STAGE

The analysis presented in this paper will give an estimate of the impact which Fox–Wolfram moments computed from jets can have on current and future LHC Higgs analyses. Fox–Wolfram moments are one way to systematically evaluate angular correlations between jets in terms of spherical harmonics. While such approaches are standard for example in cosmology, they are largely missing in LHC physics. We will summarize their main features below. For a more detailed account of the WBF-specific properties we refer to an earlier paper [20].

To allow for significant correlations between different moments we employ multivariate methods. Our analysis will largely be based on boosted decision trees (BDTs), which we will also briefly introduce below. Part of the analysis we cross–check with a neural net to make sure our findings are independent of the MVA method used.

A. Fox–Wolfram moments

Most analyses of QCD jets at the LHC are based on an *ad-hoc* selection of angular correlation variables, which have been shown to separate signals from backgrounds. For analyses where each one–dimensional or two–dimensional distribution is carefully understood in terms of the underlying physics and then tuned to the best cut value, this approach is natural and appropriate. For multivariate analyses, where events are classified in terms of a more generic set of kinematic observables, the choice of observables should be more systematic.

For angular correlations, we know how to generally describe underlying objects, in our case jets, in terms of spherical harmonics. Obviously, Fox–Wolfram moments do not have to be based on jets. They are closely related to event shapes [22], and for example at LEP they were based on calorimeter information. At the LHC, particle flow objects or topoclusters might eventually turn out more useful. In this analysis we use jets to avoid additional experimental or theoretical complications, for example due to pile-up or underlying event.

Fox–Wolfram moments are constructed by summing jet–jet correlations over all $2\ell+1$ directions, including an unspecified weight function W_i^x [19]

$$H_\ell^x = \frac{4\pi}{2\ell+1} \sum_{m=-\ell}^{\ell} \left| \sum_{i=1}^{N} W_i^x \, Y_\ell^m(\Omega_i) \right|^2 . \tag{1}$$

The index i sums over all final state jets defined by appropriate acceptance and selection criteria. The general coordinates of the spherical harmonics $Y_\ell^m(\theta,\phi)$ we replace by a reference angle Ω. The moments can be rewritten as

$$H_\ell^x = \sum_{i,j=1}^{N} W_{ij}^x \, P_\ell(\cos\Omega_{ij}) \qquad \text{with} \quad W_{ij}^x = W_i^x W_j^x . \tag{2}$$

The angle Ω_{ij} is the total angle between two jets. The weight function W_{ij}^x can be chosen freely. In Sections III and IV we will use transverse–momentum and unit weights [20]:

$$W_{ij}^T = \frac{p_{Ti}\, p_{Tj}}{\left(\sum p_{Ti}\right)^2} \qquad W_{ij}^U = \frac{1}{N^2} . \tag{3}$$

The advantage of the transverse–momentum weight is that soft and collinear jets with their limited amount of information about the hard process are automatically suppressed. The resulting analysis becomes stable with respect to the parton shower and QCD jet radiation. For tagging jets without an actual collinear divergence the transverse momentum weight should be appropriate.

Whenever we are interested in the color structure of the event, this jet radiation will carry the crucial information. For studies of central jet radiation we therefore expect the unit weight to be the most promising.

In analogy to a jet veto, Fox–Wolfram moments with unit weight introduce an energy or momentum scale, above which we include jets in the moments. Because of the unit weight there does not exist a smooth transition regime; requiring any Fox–Wolfram moment of such additional jets to be different from zero corresponds to a step function in counting the number of jets. Because the new momentum scale usually resides below the factorization scale of the hard event, fixed–order precision predictions are not applicable, and a dedicated resummation is a theoretical challenge [13–18]. In Section V we introduce the *matched weight*

$$W_{ij}^M = \frac{\left(p_{Ti} - p_T^{\min}\right)\left(p_{Tj} - p_T^{\min}\right)}{\left(\sum p_{Ti} - p_T^{\min}\right)^2} \tag{4}$$

in order to reduce the theoretical uncertainty in comparing measured cross sections to QCD predictions. This new weight avoids introducing a new hard scale and will be less dominated by the momentum scale $p_{Tj}^{\min} = 20$ GeV, above which jets contribute to the Fox–Wolfram moments.

B. Event generation

While the description of the tagging jets in weak boson fusion is straightforward, the continuum background with its QCD jet activity is more tricky. Moreover, the correct description of the QCD activity in the Higgs signal requires a careful treatment of the color structure of the hard process. Throughout this analysis we use SHERPA [24] with CKKW merging [25]. For the weak boson fusion signal we generate samples including up to three hard jets, including the tagging jets. Gluon fusion Higgs production we simulate with up to three hard jets. For the QCD background we include di–photon production plus up to two hard jets. For jet clustering we rely on the anti-k_T algorithm as in FASTJET [26] with $R = 0.4$.

The assumed Higgs mass value is 126 GeV. Our cuts are dominated by the detector acceptance and jet–photon separation,

$$p_{T\gamma} > 14 \text{ GeV} \qquad R_{\gamma j} > 0.3 \qquad m_{\gamma\gamma} > 80 \text{ GeV} . \tag{5}$$

After those cuts we are left with a weak–boson–fusion signal cross section times branching ratio of 5.2 fb at 8 TeV collider energy and 9.24 fb at 13 TeV collider energy. To allow for an efficient generation of background events we do not require a mass window for the two photons in the background generation. Later in the analysis we add an $m_{\gamma\gamma}$ window of ± 10 GeV around the Higgs mass. For a proper Higgs analysis we should require an $m_{\gamma\gamma}$ window of 1-2 GeV around the measured Higgs mass. However, with this condition the event generation for the background becomes highly inefficient. Because our analysis does not intend to predict the actual signal and background cross sections and instead focuses on the improvement over the established experimental analysis [27], the loose cuts of Eq.(5) allow for a much more efficient event generation and will not affect our conclusions.

C. Boosted decision trees

Any multivariate analysis is based on some kind of mapping of a set of observables onto a single–valued quantity, the classifier response. Based on this classifier response we define a classification rule to separate signal and background events. Training the multivariate analysis on a set of simulated events aims to determine the best classification rule for a given signal and background. The optimal classification rule has to be determined by some measure, for example the signal efficiency, the statistical significance, or the signal–to–background ratio. Independent of this optimization, we can quantify the performance of any classification rule in terms of the signal efficiency and the background mis-identification probability. In this two–dimensional plane we can describe cuts on the same response parameter as a receiver operating characteristics (ROC) curve. Given such a ROC curve we are free to choose one or more operating points. In line with the ATLAS di-photon analysis we use a fixed 40% signal efficiency ϵ_S after acceptance with a variable background rejection $1 - \epsilon_B$ as the standard working point. In Section IV, we quote the main results of our BDT analysis for the best possible significance $S/\sqrt{S+B}$ given the set of kinematic observables and Fox–Wolfram moments.

Decision tree algorithms — as they are utilized in high energy physics applications — are based on a set of kinematic variables, intended to separate signal and background events. In the first step they choose the 'root node' variable, *i.e.* the variable with the best separation between signal and background. There exist several types of separation which we can choose from in TMVA [23]. We use the cross entropy

$$C_E = -\frac{S}{S+B} \log_2 \frac{S}{S+B} - \frac{B}{S+B} \log_2 \frac{B}{S+B} , \tag{6}$$

where S and B are the numbers of signal and background events in a particular subset of events. This measure is the closest to the original definition of information entropy [28]. After choosing the root node, the subsequent nodes are ordered by their separation at some threshold value.

For the complete decision tree the events are classified as signal–like or background–like by some measure. In the training set we know how good the tree is at classifying the events. Our training set include 100000 events for each signal and background channel. In the next step the algorithm corrects for mistakes through a reweighting procedure, builds another decision tree, tests its performance, and repeats for some user–defined number of iterations. For this 'boosting' procedure we mainly use the adaptive boost algorithm implemented in

TMVA [23]. The final classification rule for signal versus background events we then apply to an independent event sample, again including 100000 events per signal and background process. To prevent over–training we limit our forest to 400 trees, and the individual trees to three layers.

Because correlations between the different Fox–Wolfram moments are a key issue of our systematic approach to kinematic input variables, we carefully test two different boosting algorithms (adaptive and gradient boost [23]) as well as different multivariate analysis methods. *Per se*, boosted decision trees are not particularly well suited for studying strongly correlated variables. The reason is that trees are built out of the individual variables. Two strongly correlated variables are best mapped through individual fine binnings in each of them, so a careful mapping of correlations will eventually lead to statistical limitations and a possible training on statistical fluctuations. Therefore, we compare BDT results to results using a multi–layer perceptron (MLP) neural network whenever an independent test appears sensible. We utilize a MLP neural network with a single hidden layer containing $N + 5$ neurons, where N is the number of training variables.

III. TAGGING JET CORRELATION

In this first analysis we are going to use Fox–Wolfram moments to systematically test the completeness of the tagging jet correlations included by ATLAS. Because we directly refer to the current ATLAS result we use a collider energy of 8 TeV for the most recent LHC run. The two p_T-ordered tagging jets have to fulfill either of the two conditions

$$\begin{aligned} p_{Tj} &> 25 \text{ GeV} \quad \text{for} \quad |y_j| < 2.4 \\ p_{Tj} &> 30 \text{ GeV} \quad \text{for} \quad 2.4 \leq |y_j| < 4.5 \,. \end{aligned} \tag{7}$$

These two tagging jets must also pass

$$|\Delta y_{j_1 j_2}| \geq 2 \quad \text{and} \quad m_{j_1 j_2} > 150 \text{ GeV} \,. \tag{8}$$

These cuts correspond to the variables used in the multivariate di-photon Higgs analysis by ATLAS [27],

$$\{m_{j_1 j_2} \,,\, y_{j_1} \,,\, y_{j_2} \,,\, \Delta y_{j_1 j_2}\} \qquad \text{(ATLAS default)}. \tag{9}$$

The angular correlations between the tagging jets in weak–boson–fusion Higgs production is known to reflect the tensor structure of the WWH vertex [21]. In this application the collinearity of the two tagging jets plays an important role, with the effect that the azimuthal angle between the tagging jet is a more sensitive probe than the opening angle between them. For the Fox–Wolfram moments this means that the definition in terms of the opening angle Ω_{ij} is not optimally suited. For the tagging jet analysis we therefore replace the opening angle in the Legendre polynomials by the azimuthal angle $\Delta\phi_{ij}$ between the two tagging jets,

$$H_\ell^{x,\phi} = \sum_{i,j=1}^{2} W_{ij}^x \, P_\ell(\cos \Delta\phi_{ij}) \,. \tag{10}$$

For a systematic study of the usefulness of the tagging jet correlations we perform a multi-variate analysis of the Fox–Wolfram moments introduced in Section II A. Because the moments are based on spherical harmonics they form a basis and include all available information, given the weight W_{ij}^x we use in their definition.

We show some sample BDT and MLP results based on the azimuthal moments in Table I. The full set of moments for each weight function by definition includes all available information for the corresponding weights. First, we see that including a large set of Fox–Wolfram moments gives a significant improvement of the current ATLAS set of observables, defined in Eq.(9). Both multivariate analyses using the first four moments with unit weight as well as with transverse–momentum weight reduces the remaining fraction of background events by a factor two. From the TMVA output we have checked that these eight moments dominate the distinctive power of the analysis.

Obviously, the next question is which of the Fox–Wolfram moments contribute most to this improvement. From the earlier analysis [20] we know that lower moments will dominate in the tagging jet analysis, and that only odd moments can distinguish between forward–backward and forward–forward tagging jets. Individually,

	BDT			MLP		
$\epsilon_S = 0.4$	$1-\epsilon_B$	$\frac{S}{\sqrt{S+B}}$	$\frac{S}{B}$	$1-\epsilon_B$	$\frac{S}{\sqrt{S+B}}$	$\frac{S}{B}$
ATLAS default Eq.(9)	0.887	1.50	0.76	0.888	1.50	0.78
$H_1^{T,\phi} \to H_4^{T,\phi}$, $H_1^{U,\phi} \to H_4^{U,\phi}$	0.952	1.65	1.54	0.953	1.65	1.55
$H_1^{T,\phi}$, $H_3^{T,\phi}$, $H_1^{U,\phi}$, $H_3^{U,\phi}$	0.952	1.66	1.56	0.952	1.65	1.54
$H_1^{T,\phi}$, $H_2^{T,\phi}$, $H_2^{U,\phi}$, $H_2^{U,\phi}$	0.953	1.65	1.47	0.953	1.65	1.55
$H_1^{T,\phi}$, $H_1^{U,\phi}$	0.953	1.65	1.43	0.952	1.65	1.46
$H_1^{T,\phi}$	0.950	1.63	1.45	0.950	1.63	1.44
$H_1^{U,\phi}$	0.952	1.65	1.40	0.952	1.65	1.44
$\cos\Delta\phi_{12}$, W_{12}^T	0.952	1.65	1.53	0.952	1.65	1.50
$\cos\Delta\phi_{12}$	0.952	1.65	1.42	0.952	1.65	1.44

Table I: BDT and MLP results including azimuthal–angle Fox–Wolfram moments based on the two tagging jets only after Eq.(8). The background rejection is given for 40% signal efficiency. The value for $S/\sqrt{S+B}$ we compute for an integrated luminosity of 30 fb^{-1}. All sets of variables subsequent to the first row contain the default variables as well.

we find that the six best individual moments are (in order) $H_1^{U,\phi}$, $H_1^{T,\phi}$, $H_3^{U,\phi}$, $H_3^{T,\phi}$, $H_2^{U,\phi}$, and $H_2^{T,\phi}$.* The moments with unit weight are slightly more powerful than the transverse–momentum weight. The most striking feature is that for the tagging jet the higher moments play hardly any role in improving the analysis.

As a matter of fact, the single moment $H_1^{U,\phi}$ is, within uncertainties due to the training procedure, almost as powerful as the set of the first 20 moments, both with unit and transverse–momentum weight. Given that the corresponding Legendre polynomial is $P_1(\cos\Delta\phi_{ij}) = \cos\Delta\phi_{ij}$ we can further simplify the analysis by separating the transverse–momentum weight from the azimuthal angle. Compared to the ATLAS default variables, adding the azimuthal angle between the tagging jets, $\Delta\phi_{ij}$, almost doubles the signal–to–background ratio. Systematically including the Fox–Wolfram moments increases the signal–to–background ratio additionally by 8%. This result persists between the two multivariate methods and we conclude that our improvement is truly due to the nature of the moments and not to some advantageous choice of methods and/or parameters for our multivariate analyses.

Following the tagging jet analysis in this section we extend the default set of tagging jet cuts Eq.(9) for the remainder of this paper to include

$$\{m_{j_1 j_2}\,,\, y_{j_1}\,,\, y_{j_2}\,,\, \Delta y_{j_1 j_2},\, \Delta\phi_{j_1 j_2}\} \qquad \text{(WBF default)}. \tag{11}$$

It could be argued that adding the azimuthal angle to the list of kinematic variables employed in the background rejection will make the analysis result less applicable to modified Higgs–like signal hypotheses. Indeed, the azimuthal angle between the tagging jets is the key observable in the spin-0 CP analysis of the Higgs resonance [21]. On the other hand, the same is true for the rapidity difference Δy_{12} when it comes to spin-2 alternatives [21].

IV. REPLACING A JET VETO

The key physics question we will answer in this Section is to what degree we can use information on additional (central) jet radiation to enhance the tagging jet analysis described in the previous Section III. Because a detailed analysis of the jet activity has not been performed in the recent LHC runs, we assume a collider energy of 13 TeV in this section. The physics of the additional jets can be easily described: for the signal events the emission of additional central jets is suppressed by the color structure of the process. This means that the number of jets in weak boson fusion will in general follow the staircase pattern predicted for inclusive processes at the LHC [13]. In contrast, gluon–fusion Higgs production or di-photon production will show this staircase pattern only in the absence of tagging jet cuts. Once we require two hard jets with a large invariant mass we induce large logarithms,

* Given that TMVA gives an ordered list of the most relevant observables, it is not clear to one of the authors (TP) why this very interesting information is never shown in experimental publications.

	Δy-selection			p_T-selection		
	WBF	GF	$\gamma\gamma$	WBF	GF	$\gamma\gamma$
generated [fb]	6.5	4.5	2050	6.5	4.5	2050
$\Delta y_{j_1 j_2} > 4.4$	$\times 0.33$	$\times 0.15$	$\times 0.11$	$\times 0.27$	$\times 0.056$	$\times 0.055$
$y_{j1} y_{j2} < 0.0$	$\times 1.00$	$\times 1.00$	$\times 1.00$	$\times 1.00$	$\times 1.00$	$\times 1.00$
$m_{j_1 j_2} > 600$ GeV	$\times 0.72$	$\times 0.55$	$\times 0.46$	$\times 0.77$	$\times 0.61$	$\times 0.47$
cut level [fb]	1.52	0.37	107	1.36	0.15	52.9
central jet veto	$\times 0.75$	$\times 0.15$	$\times 0.22$	$\times 0.91$	$\times 0.45$	$\times 0.52$
veto level [fb]	1.14	0.056	24.0	1.24	0.068	27.7

Table II: Cut flow for the standard weak–boson–fusion analysis with a central jet veto for an LHC energy of 13 TeV.

which leads to a Poisson pattern in the number of jets [13]. The key feature of this Poisson distribution is a significantly enhanced probability of radiating a central jet.

Throughout our analysis we require two tagging jets with the generic acceptance cuts

$$p_{Tj} > 20 \text{ GeV} \qquad |y_j| < 4.5 \tag{12}$$

$$|\Delta y_{j_1 j_2}| > 2 \qquad m_{j_1 j_2} > 150 \text{ GeV} . \tag{13}$$

Correspondingly, we generate signal and background events using Sherpa [24] with CKKW [25] jet merging with two or three hard jets from the matrix element. Throughout this Section we assume a collider energy of 13 TeV. In addition to the general photon cuts of Eq.(5) we require $m_{\gamma\gamma} = 126 \pm 10$ GeV. The cuts of Eq. (12) lead to cross sections of 6.5 fb for the weak–boson–fusion signal, 4.5 fb for gluon–fusion Higgs production, and 2050 fb for the continuum background. As mentioned above, the signal–to–background ratio can be improved through additional cuts, such as tightening the $m_{\gamma\gamma}$ requirement. However, this makes it harder to reliably simulate the background. In the following we will assume that additional cuts on the Higgs decay products are orthogonal to the additional jet kinematics.

Because the selection criterion of the two tagging jets has a significant impact on the amount of Poisson enhancement of the additional jet production we use two selection criteria for the tagging jets:

1. p_T-selection: of all jets fulfilling Eqs.(12) and (13) the two hardest are the tagging jets. The mild cuts of Eq.(13) leave 3.36 fb for the signal, 1.04 fb for gluon–fusion Higgs production, and 509 fb for the continuum background.

2. Δy-selection: of all jets fulfilling Eq.(12) and (13) the two most forward and backward are the tagging jets, maximizing $\Delta y_{j_1 j_2}$. After Eq.(13) the remaining rates are 3.78 fb for the signal, 1.71 fb for gluon–fusion Higgs production, and 736.2 fb for the non-Higgs background.

While the p_T-selection is standard in most weak–boson–fusion analyses, it will turn out that the Δy-selection is more efficient in generating a large Poisson enhancement for central jet emission in the background processes. On the other hand, in particular for the 13 TeV run we have to see if pile-up makes one of the two selections appear experimentally superior.

The standard approach to including the additional jet activity in the weak–boson–fusion Higgs analysis is a central jet veto [12, 15]. To generate a sufficiently strong Poisson pattern in the number of jets we demand

$$|\Delta y_{j_1 j_2}| > 4.4 \qquad y_{j1} \cdot y_{j2} < 0 \qquad m_{j_1 j_2} > 600 \text{ GeV} . \tag{14}$$

In Table II we show the cut flow of the signal and background rates for each step in Eq.(14). Finally, we include a central jet veto which does not allow for jets above $p_T = 20$ GeV in between the two tagging jets. While the two tagging jet selections show significant differences in the intermediate steps, after the veto the numbers of signal and background events are comparable. The survival rates for the central jet veto are in agreement with the literature [7, 15].

In the first three rows of Table III we show different statistical measures after the acceptance cuts of Eqs.(12) and (13), the veto–level cuts of Eq.(14), and after the central jet veto. The background is composed of gluon–fusion Higgs production and continuum di-photon production. We again see that the significance $S/\sqrt{S+B}$ and the signal–to–background ratio are comparable for the Δy-selection and the p_T-selection of the tagging jets.

	Δy-selection				p_T-selection			
	ϵ_S	$1-\epsilon_B$	$\frac{S}{\sqrt{S+B}}$	$\frac{S}{B}$	ϵ_S	$1-\epsilon_B$	$\frac{S}{\sqrt{S+B}}$	$\frac{S}{B}$
acceptance cuts Eqs.(12) and (13)	1	0	0.76	0.005	1	0	0.81	0.007
veto–level cuts Eq.(14)	0.402	0.854	0.80	0.014	0.405	0.996	1.01	0.026
jet veto	0.302	0.967	1.24	0.047	0.369	0.945	1.26	0.045
BDT: WBF default with Eq.(13)	0.400	0.862	0.79	0.014	0.400	0.904	1.04	0.027
	0.634	0.674	0.84	0.010	0.414	0.897	1.04	0.027
BDT: WBF default plus FWM with Eq.(13)	0.400	0.952	1.34	0.041	0.400	0.944	1.35	0.047
	0.232	0.986	1.42	0.083	0.302	0.972	1.43	0.071

Table III: S/B and $S/\sqrt{S+B}$ compared to classical cut and jet veto strategy for the Δy and p_T-selections of the tagging jets. The value for $S/\sqrt{S+B}$ we compute for an integrated luminosity of 30 fb^{-1}. The BDT analysis includes a set of Fox–Wolfram moments with unit weight, Eq.(15). We quote two working points at 40% signal efficiency and optimized for $S/\sqrt{S+B}$.

However, this is only true after the jet veto. After only the hard cuts of Eq.(14) the p_T-selection is significantly more promising. As alluded to above, the jet veto benefits from the stronger Poisson enhancement from the Δy-selection, leaving the final results essentially identical.

In the next step, we use the default WBF observables of Eq.(11) and optimize them in a multivariate BDT analysis as described in Section II C. The corresponding ROC curve we show in Figure 1. As in Table III the efficiencies are defined with respect to the full set of acceptance cuts from Eqs.(12) and (13). In the table we quote two points from this curve. First, we show the usual working point with a signal efficiency of 40%. Second, we show the working point with the best result for $S/\sqrt{S+B}$. Optimizing for the best result of S/B does not give a well defined solution. As expected, the ROC curve indicates working points for the entire range of signal efficiencies $\epsilon_S = 0...1$.

The question we attempt to answer in this section is if we can use the available information on the additional jet activity in reducing the two backgrounds more efficiently than with a central jet veto. The baseline for this comparison is the corresponding row in Table III. As described in Section II A we rely on a large set of Fox–Wolfram moments forming a basis for the angular correlations given a weight W_{ij}^x. Unlike for the tagging jet kinematics we now do not constrain our system to the transverse plane, which means we use the original definition of the moments in Eq.(2) with the opening angle Ω_{ij}. On the other hand, we already know what the benefit of including the moments of the tagging jets are: according to Section III most of the information is included once we add the azimuthal angle between the tagging jets, $\Delta\phi_{j_1 j_2}$, to the standard set of observables given in Eq.(11). Therefore, we limit the analysis of the additional jet activity to all jet–jet correlations *with the exception of the two tagging jets*. Moreover, we can expect the unit weight to give the best sensitivity to the relatively soft additional jet activity, so we use

$$H_\ell^U = \frac{1}{N^2} \sum_{(i,j)\neq(1,2)} P_\ell(\cos\Omega_{ij}) \; . \tag{15}$$

For both of the tagging jet selections we only include jets which fall between the two tagging jets, in complete analogy of a central jet veto. For exactly two tagging jets and no additional jet radiation this implies $H_\ell^U = 0$ for all values of ℓ.

In Table III we show the result of a combined BDT analysis of the observable of Eq.(11) and the set of Fox–Wolfram moments. Again, we quote two operating points, one of them for a fixed signal efficiency of 40% and one optimized for the best value of $S/\sqrt{S+B}$. In addition, we show results for both, the Δy-selection and the p_T-selection of the tagging jets. A generic problem for any BDT analysis is that for limited statistics of the training sample it can only include a limited number of observables. On the other hand, the BDT first determines the most powerful observables, so we only include the five best Fox–Wolfram moments in our analysis. We have checked that adding more moments will not improve the result beyond numerical accuracy. For the Δy-selection the five leading moments with unit weight are H_2^U, H_4^U, H_{18}^U, H_{19}^U, and H_{17}^U. For the p_T-selection the most powerful moments are H_2^U, H_{19}^U, H_{17}^U, H_{20}^U, and H_{15}^U. However, for the p_T-selection the most powerful variable in the BDT is $\Delta y_{j_1 j_2}$. For the Δy-selection this observable is maximized by construction.

The ROC curves in Figure 1 shows a clear improvement of the complete multivariate analysis including the Fox–Wolfram moments as compared to the kinematic variables of Eq.(11) only. For a fixed moderate signal

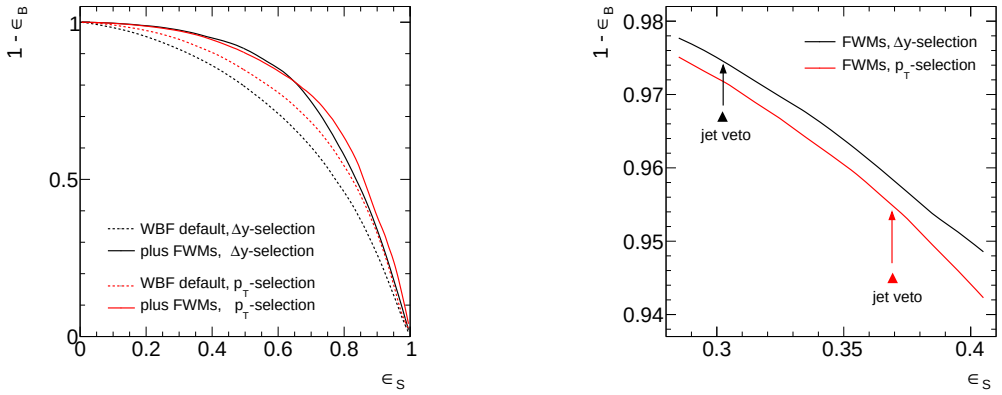


Figure 1: ROC curve for Δy- (black) and p_T-selection (red) of the tagging jets. Left: We compare the WBF default observables (dashed) of Eq.(11) to an additional set of Fox–Wolfram moments (solid). Right: We show how using Fox–Wolfram moments compare to a central jet veto.

efficiency of 40% adding information on the jets decreases the probability of a background mis-identification by a factor of 2.9 for the Δy-selection and a factor of 1.7 for the p_T-selection. The improvement relative to the jet veto we show in the right panel, zooming into typical signal efficiencies around 35% relative to the acceptance cuts of Eq.(13). For the jet veto working point of the Δy-selection with fixed signal efficiency of 30.2% we see that the background misidentification is reduced by 30%. For the p_T-selection with fixed signal efficiency of 36.9% we find an improvement by 20%.

V. AVOIDING NEW SCALES

The unit weights in the definition of the Fox–Wolfram moments used in the previous Section IV share a disadvantage with a jet veto when it comes to predicting them from theory: they introduce an additional physical momentum scale in the process which is below the hard scale of the Higgs production process. Collinear factorization as the basis of defining the parton densities in perturbative field theory does not allow for such additional scales. All measurements which are to be compared to fixed–order perturbative QCD predictions have to be jet–inclusive for transverse momenta below the factorization scale. If we introduce an additional scale this implies that we introduce a possibly large logarithm which needs to be resummed [16–18].

Introducing a weight which smoothly interpolates between the jet counting scale $p_{Tj}^{\min} = 20$ GeV and the hard scale of the process according to Eq.(4) should alleviate this tension, suggesting to repeat the same analysis as shown in Section IV with the Fox–Wolfram moments

$$H_\ell^M = \sum_{(i,j)\neq(1,2)} \frac{(p_{Ti} - p_T^{\min})\,(p_{Tj} - p_T^{\min})}{\left(\sum p_{Ti} - p_T^{\min}\right)^2}\, P_\ell(\cos\Omega_{ij})\ . \tag{16}$$

	Δy-selection				p_T-selection			
	ϵ_S	$1-\epsilon_B$	$\frac{S}{\sqrt{S+B}}$	$\frac{S}{B}$	ϵ_S	$1-\epsilon_B$	$\frac{S}{\sqrt{S+B}}$	$\frac{S}{B}$
jet veto Eq.(12) to (14)	0.302	0.967	1.24	0.047	0.369	0.945	1.26	0.045
BDT: WBF default plus unit–weight FWM	0.400	0.952	1.34	0.041	0.400	0.944	1.35	0.047
	0.232	0.986	1.42	0.083	0.302	0.972	1.43	0.071
BDT: WBF default plus matched–weight FWM	0.400	0.949	1.32	0.040	0.400	0.942	1.32	0.045
	0.240	0.985	1.43	0.081	0.256	0.979	1.40	0.082

Table IV: S/B and $S/\sqrt{S+B}$ compared to jet veto strategy for the Δy and p_T-selections of the tagging jets. The value for $S/\sqrt{S+B}$ we compute for an integrated luminosity of 30 fb^{-1}. Extending Table III the BDT analysis now includes a set of Fox–Wolfram moments with matched weight, Eq.(16). As BDT results we quote the working point at 40% signal efficiency and the best point for $S/\sqrt{S+B}$.

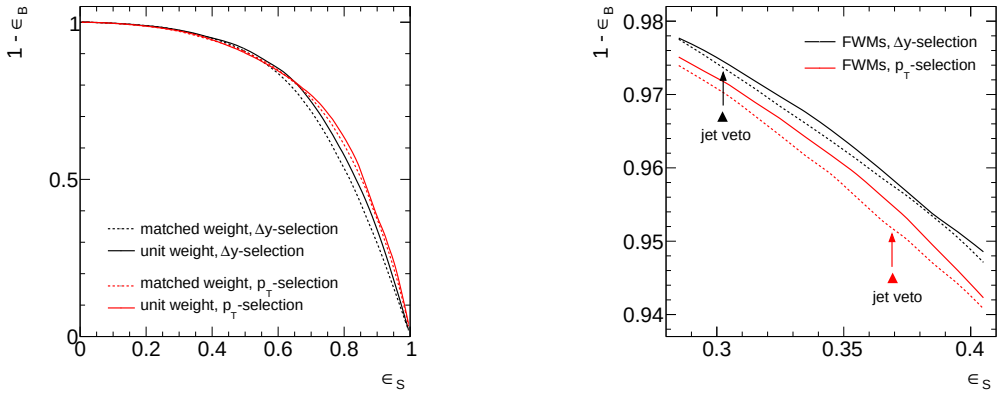


Figure 2: ROC curve for Δy- (black) and p_T-selection (red) of the tagging jets. Left: We compare the WBF default observables (dashed) of Eq.(11) to an additional set of Fox–Wolfram moments (solid). Right: We show how using Fox–Wolfram moments compares to a central jet veto.

While we cannot offer an estimate of the improvement in the perturbative QCD treatment, it is clear that the matched weights are less sensitive to large collinear logarithms generated by the violation of collinear factorization.

In Table IV we extend the original Table III, including the same BDT analysis now based on matched Fox–Wolfram moments. For the standard working point with 40% signal efficiency we see that the background rejection from the matched moments is essentially identical to the unit weight moments. The main difference is the order of the most relevant set of moments, which now is $H_1^M, H_2^M, H_3^M, H_4^M, H_6^M$ for the Δy-selection and $H_1^M, H_3^M, H_6^M, H_2^M, H_4^M$ for the p_T-selection. Similarly, the working point optimized for $S/\sqrt{S+B}$ is only slightly shifted. In Figure 2 we compare the ROC curves for the jet radiation study based on the two Fox–Wolfram moment weights. For signal efficiencies between 25% and 40% the unit weight is slightly superior, but most likely this slight advantage will be compensated once we include theory uncertainties from QCD predictions.

VI. OUTLOOK

Weak boson fusion analyses of Higgs production at the LHC are key ingredients to Higgs couplings and Higgs property analyses in the upcoming LHC run. They allow for an efficient background rejection based on two tagging jets and an additional central jet veto. The question is, how we can make optimal use of the jet properties for example to improve the signal–to–background ratio or the signal significance. In our detailed analysis we come to three conclusions:

1. For the two tagging jets we rely on a set of low-ℓ moments with a transverse momentum weight and azimuthal angle separation. Most of the improvement as compared to the standard ATLAS analysis can be traced back to the missing azimuthal angle between the tagging jets. In addition, the signal–to–background ratio can be increased by 8% by including a set of Fox–Wolfram moments.

2. The additional jets can be studied using a wide range of moments with a unit weight and full angular separation. It should be compared to a jet veto and delivers a significantly better performance. The tagging jet selection with maximum rapidity distance is better suited to distinguish the signal from the continuum background then the transverse momentum selection. For both cases we computed a full ROC curve, allowing for optimized working points depending on the details of the analysis.

3. To reduce theory uncertainties from QCD predictions we can introduce a softer, matched weight in the Fox–Wolfram moments. It turns out that the analysis of jet radiation is almost as promising as for the unit weights, but with a much improved theoretical behavior.

We conclude that tagging jet criteria as well as the jet veto as analysis tools for Higgs analyses in weak boson fusion can be improved by a systematic study of the multi–jet system based on Fox–Wolfram moments. The improvement is significant, both for the Δy-selection and the p_T-selection of the tagging jets. The Fox–Wolfram moment analysis can be adapted to individual analyses by choosing appropriate working points in the corresponding ROC curves.

Acknowledgments

CB would like to thank the ATLAS collaboration at CERN, where part of this work was performed. We would like to thank Erik Gerwick and Steffen Schumann for help with the event generation. CB acknowledges support by BMBF under project number 05H12VHE. PS acknowledges support by the IMPRS for *Precision Tests of Fundamental Symmetries*.

[1] P. W. Higgs, Phys. Lett. **12**, 132 (1964); P. W. Higgs, Phys. Rev. Lett. **13**, 508 (1964); F. Englert and R. Brout, Phys. Rev. Lett. **13**, 321 (1964).
[2] G. Aad *et al.* [ATLAS Collaboration], Phys. Lett. B **716**, 1 (2012).
[3] S. Chatrchyan *et al.* [CMS Collaboration], Phys. Lett. B **716**, 30 (2012).
[4] G. Weiglein *et al.* [LHC/LC Study Group Collaboration], Phys. Rept. **426**, 47 (2006); M. Klute, R. Lafaye, T. Plehn, M. Rauch and D. Zerwas, Europhys. Lett. **101**, 51001 (2013).
[5] see *e.g.* M. Shaposhnikov and C. Wetterich, Phys. Lett. B **683**, 196 (2010); M. Holthausen, K. S. Lim and M. Lindner, JHEP **1202**, 037 (2012); A. Hebecker, A. K. Knochel and T. Weigand, Nucl. Phys. B **874**, 1 (2013) D. Buttazzo *et al* arXiv:1307.3536 [hep-ph];
[6] for up-to-date coupling analyses see [ATLAS Collaboration], ATLAS-CONF-2013-034; [ATLAS Collaboration], ATLAS-CONF-2013-040; [CMS Collaboration], CMS-PAS-HIG-13-005; T. Plehn and M. Rauch, Europhys. Lett. **100**, 11002 (2012); D. Lopez-Val, T. Plehn and M. Rauch, JHEP **1310**, 134 (2013); T. Corbett, O. J. P. Eboli, J. Gonzalez-Fraile and M. C. Gonzalez-Garcia, arXiv:1306.0006 [hep-ph]; I. Brivio *et al* arXiv:1311.1823 [hep-ph]. A. Azatov, R. Contino and J. Galloway, JHEP **1204**, 127 (2012); J. Ellis and T. You, JHEP **1306**, 103 (2013); G. F. Giudice, C. Grojean, A. Pomarol and R. Rattazzi, JHEP **0706**, 045 (2007); J. R. Espinosa, C. Grojean, M. Mühlleitner and M. Trott, JHEP **1212**, 045 (2012); S. Banerjee, S. Mukhopadhyay and B. Mukhopadhyaya, JHEP **1210**, 062 (2012); N. Craig and S. Thomas, JHEP **1211**, 083 (2012); F. Bonnet, T. Ota, M. Rauch and W. Winter, Phys. Rev. D **86**, 093014 (2012); A. Djouadi, arXiv:1208.3436 [hep-ph]; B. A. Dobrescu and J. D. Lykken, JHEP **1302**, 073 (2013); E. Massó and V. Sanz, Phys. Rev. D **87**, 033001 (2013); G. Belanger, B. Dumont, U. Ellwanger, J. F. Gunion and S. Kraml, JHEP **1302**, 053 (2013); P. P. Giardino, K. Kannike, I. Masina, M. Raidal and A. Strumia, arXiv:1303.3570 [hep-ph]; A. Djouadi and G. Moreau, arXiv:1303.6591 [hep-ph]; D. Carmi, A. Falkowski, E. Kuflik, T. Volansky and J. Zupan, JHEP **1210**, 196 (2012); P. P. Giardino, K. Kannike, I. Masina, M. Raidal and A. Strumia, arXiv:1303.3570 [hep-ph];
[7] D. L. Rainwater, D. Zeppenfeld and K. Hagiwara, Phys. Rev. D **59**, 014037 (1999); T. Plehn, D. L. Rainwater and D. Zeppenfeld, Phys. Rev. D **61**, 093005 (2000).
[8] N. Kauer, T. Plehn, D. Rainwater and D. Zeppenfeld, Phys. Lett. B **503**, 113 (2001).
[9] D. L. Rainwater and D. Zeppenfeld, JHEP **9712**, 005 (1997); J. R. Andersen, C. Englert and M. Spannowsky, arXiv:1211.3011 [hep-ph].
[10] S. Asai, G. Azuelos, C. Buttar, V. Cavasinni, D. Costanzo, K. Cranmer, R. Harper and K. Jakobs *et al.*, Eur. Phys. J. C **32S2**, 19 (2004).
[11] for LHC reviews *e.g.* A. Djouadi, Phys. Rept. **457**, 1 (2008); T. Plehn, Lect. Notes Phys. **844**, 1 (2012) [arXiv:0910.4182 [hep-ph]].
[12] R. Kleiss and W. J. Stirling, Phys. Lett. B **200**, 193 (1988); U. Baur and E. W. N. Glover, Phys. Lett. B **252**, 683 (1990); V. D. Barger, K. Cheung, T. Han, J. Ohnemus and D. Zeppenfeld, Phys. Rev. D **44**, 1426 (1991).
[13] E. Gerwick, T. Plehn and S. Schumann, Phys. Rev. Lett. **108**, 032003 (2012); E. Gerwick, T. Plehn, S. Schumann and P. Schichtel, JHEP **1210**, 162 (2012); E. Gerwick, S. Schumann, B. Gripaios and B. Webber, JHEP **1304**, 089 (2013).
[14] B. E. Cox, J. R. Forshaw and A. D. Pilkington, Phys. Lett. B **696**, 87 (2011).
[15] D. L. Rainwater, R. Szalapski and D. Zeppenfeld, Phys. Rev. D **54**, 6680 (1996).
[16] T. Becher and M. Neubert, JHEP **1207**, 108 (2012); T. Becher, M. Neubert and L. Rothen, JHEP **1310**, 125 (2013).
[17] A. Banfi, G. P. Salam and G. Zanderighi, JHEP **1206**, 159 (2012) A. Banfi, P. F. Monni, G. P. Salam and G. Zanderighi, Phys. Rev. Lett. **109**, 202001 (2012).
[18] I. W. Stewart and F. J. Tackmann, Phys. Rev. D **85**, 034011 (2012); I. W. Stewart, F. J. Tackmann, J. R. Walsh and S. Zuberi, arXiv:1307.1808 [hep-ph].
[19] G. C. Fox and S. Wolfram, Phys. Rev. Lett. **41**, 1581 (1978); R. D. Field, Y. Kanev and M. Tayebnejad, Phys. Rev. D **55**, 5685 (1997).
[20] C. Bernaciak, M. S. A. Buschmann, A. Butter and T. Plehn, Phys. Rev. D **87**, 073014 (2013).
[21] T. Plehn, D. L. Rainwater and D. Zeppenfeld, Phys. Rev. Lett. **88**, 051801 (2002); C. Ruwiedel, N. Wermes and M. Schumacher, Eur. Phys. J. C **51**, 385 (2007); K. Hagiwara, Q. Li and K. Mawatari, JHEP **0907**, 101 (2009); C. Englert, D. Goncalves-Netto, K. Mawatari and T. Plehn, JHEP **1301**, 148 (2013); A. Djouadi, R. M. Godbole, B. Mellado and K. Mohan, Phys. Lett. B **723**, 307 (2013).
[22] for a nice overview of LHC applications see *e.g.* A. Banfi, G. P. Salam and G. Zanderighi, JHEP **1006**, 038 (2010).
[23] A. Höcker *et al.*, PoS ACAT , 040 (2007) [physics/0703039 [PHYSICS]]; P. Speckmayer, A. Höcker, J. Stelzer and H. Voss, J. Phys. Conf. Ser. **219**, 032057 (2010); `http://tmva.sourceforge.net`
[24] T. Gleisberg, S. Höche, F. Krauss, M. Schönherr, S. Schumann, F. Siegert and J. Winter, JHEP **0902**, 007 (2009).

[25] S. Catani, F. Krauss, R. Kuhn and B. R. Webber, JHEP **0111**, 063 (2001).
[26] M. Cacciari, G. P. Salam and G. Soyez, Eur. Phys. J. C **72**, 1896 (2012).
[27] [ATLAS Collaboration], ATLAS-CONF-2013-012.
[28] J. R. Quinlan, *C4.5: Programs for Machine Learning*, Morgan Kaufmann, San Mateo, CA (1992)